PAPER

Efficiency Analysis for Inductive Power Transfer Using Segmented Parallel Line Feeder

William-Fabrice BROU†a), *Nonmember*, **Quang-Thang DUONG**†b), ***and*** **Minoru OKADA**†c), ***Members***

SUMMARY Parallel line feeder (PLF) consisting of a two-wire transmission line operating in the MHz band has been proposed as a wide-coverage short-distance wireless charging. In the MHz band, a PLF of several meters suffers from standing wave effect, resulting in fluctuation in power transfer efficiency accordingly to the receiver's position. This paper studies a modified version of the system, where the PLF is divided into individually compensated segments to mitigate the standing wave effect. Modelling the PLF as a lossy transmission line, this paper theoretically shows that if the segments' lengths are properly determined, it is able to improve and stabilize the efficiency for all positions. Experimental results at 27.12 MHz confirm the theoretical analysis and show that a fairly high efficiency of 70% can be achieved.

key words: *parallel line feeder, standing wave problem, segmentation, efficiency stabilization, efficiency improvement*

1. Introduction

Wireless power transfer (WPT) is a promising solution to the energy problem of sensor networks when battery replacement is impractical [1]–[7]. Among major WPT techniques, microwave power transfer (MPT) [8], [9] is a radiative type of energy transmission and is suitable for charging low power sensors (∼mW) at long distance (tens of meters or longer) [10]–[13]. On the contrary, inductive power transfer (IPT) [14], [15] is a non-radiative type of energy transmission, operating on the same principle of a transformer. This technique is capable of charging higher power sensors (∼W) but at much shorter distance (up to tens of centimeters at most). Fortunately, this limitation in transmission range, to some extent, can be compensated for by a well-designed transmitting coil that covers a wide charging area. In such a case, IPT becomes a viable charging solution for stationary sensors requiring power levels far beyond the charging capability of MPT technique.

A wide coverage IPT can be realized by elongating the transmitting coil as in [14], [16] or by deploying many small coils in an array as in [17]–[21]. The coil-array is able to focus the magnetic field toward the receiving coils to achieve a sufficient coupling, but it requires a complex mechanism to locate the receivers and to activate/deactivate the coils. On the contrary, the elongated-coil has a much simpler hardware but suffers from insufficient coupling due to the imbalance in dimensions of the coils. Motivated by the simplicity of the elongated-coil, this paper addresses its weak coupling problem to achieve a sufficient efficiency for practical applications.

For a given coupling coefficient, the efficiency of IPT can be improved by increasing the Q-factors of the coils [22]–[25]. As the Q-factors can be improved by properly raising the operation frequency, the parallel line feeder (PLF) system in [26] operates in the 13.56 MHz band, which is higher than the kHz band adopted by many typical IPT systems employing the Qi standard [27]. The PLF in [26] achieves a good theoretical efficiency of about 85% but its coverage is just about 1 m long. Further elongating the feeder makes its length non-negligible compared to the signal wavelength (about 20 m). This results in fluctuation in output voltage according to receiver position due to the standing wave effect. To address this problem, we have proposed dividing the PLF into individually resonated segments [28], [29]. This paper is an extension of our previous works [28], [29] with novel contributions summarized below.

- Modelling the PLF as a lossy transmission line [30], this paper analyzes the maximum achievable efficiency [22]–[25] according to the segments' lengths. We show that if the segments' lengths are properly determined, it is able to improve and stabilize the efficiency for all receiver position. It is worth noting that efficiency analysis has not been done in [28], [29] because these investigations have not considered losses in the feeder.
- The aforementioned theoretical analysis is confirmed by extensive experiments. Our experimental results at 27.12 MHz show that the segmented PLF can stabilize the efficiency as fairly high value as 70% for all receiver positions along the feeder.

The rest of this paper is organized as follows. Section 2 presents the efficiency analysis for the non-segmented PLF system. Section 3 theoretically shows that efficiency improvement and stabilization effects can both be achieved with the segmented PLF system. Section 4 provides experimental results and Sect. 5 concludes this paper.

Manuscript received February 26, 2022.
Manuscript revised August 3, 2022.
Manuscript publicized October 17, 2022.

†The authors are with the Graduate School of Information Science, Nara Institute of Science and Technology, Ikoma-shi, 630–0192 Japan.
a) E-mail: william.brou.fab@gmail.com
b) E-mail: thang@is.naist.jp
c) E-mail: mokada@is.naist.jp

DOI: 10.1587/transele.2022ECP5013

2. Non-Segmented PLF

2.1 Theoretical Analysis

A simplified schematic of the non-segmented PLF is described in Fig. 1(a), where a two-wire transmission line of length L is connected to a radio frequency (RF) sinusoidal source via a resonant capacitor C_1 to function as the transmitter coil. The operation frequency denoted by f is in the MHz range to achieve high Q-factors. The angular frequency is $\omega = 2\pi f$, and the signal wavelength in free space is $\lambda_0 = c/f$, where c is the speed of light. As shown in the figure, the feeder consists of two parallel wires of identical diameter d separated at a distance D (center-to-center). In real applications, the feeder may be surrounded by dielectric materials. To model the surrounding dielectrics, let the propagation constant of the feeder be a complex value $\gamma = \alpha + j\beta$, where α is the attenuation constant and β is the phase constant. The attenuation constant α includes all losses in the feeder, e.g.,copper loss, dielectric loss. From a practical perspective, it is reasonable to assume that the feeder is low loss, meaning that $\alpha L \ll 1$. The phase constant β usually differs from its free space value $\beta_0 = 2\pi/\lambda_0$. Due to the dielectric effect, wavelength of the signal propagated in the feeder is $\lambda = 2\pi/\beta$, which may differ from its free space value λ_0. The ratio of these two values is equal to the refractive index of the dielectric $n = \lambda_0/\lambda$. The characteristic impedance of the feeder [31]

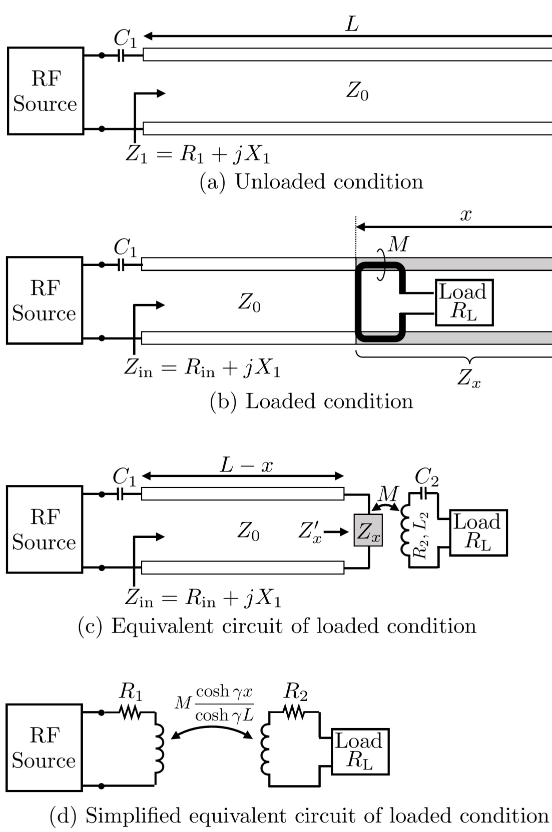

Fig. 1 System model of non-segmented PLF.

$$Z_0 = \frac{120\,\Omega}{n}\cosh^{-1}\frac{D}{d} \tag{1}$$

Without loss of generality, throughout this paper we assume that the feeder is terminated in a short circuit. In the unloaded condition in Fig. 1(a), the input impedance of the feeder is

$$Z_1 = Z_0 \tanh\gamma L = R_1 + jX_1, \tag{2}$$

where

$$R_1 = \frac{Z_0 \sinh(2\alpha L)}{\cosh(2\alpha L) + \cos(2\beta L)} \tag{3}$$

$$X_1 = \frac{Z_0 \sin(2\beta L)}{\cosh(2\alpha L) + \cos(2\beta L)} \tag{4}$$

In Eq. (2), the imaginary part jX_1 is then cancelled by the resonant capacitor $C_1 = 1/(\omega X_1)$, while the real part R_1 remains. It is worth noting that the value of R_1 alone does not accurately reflect losses in the energy transmission when the load is coupled to the feeder.

Now, let us consider the loaded condition illustrated in Fig. 1(b) when a receiver is located at the position x from the terminating end of the feeder. In this case, the feeder can be divided into two parts: the part of length x on the right-hand side coupling with the receiver's coil, and the part of length $L-x$ on the left-hand side which does not couple with the receiver. As the coupling part can be seen as a shorted transmission line of length x, its input impedance can be expressed as

$$Z_x = Z_0 \tanh(\gamma x) \tag{5}$$

Via the coupling M, the load reflects an impedance on the feeder. Let the mutual coupling between the feeder and the receiver coil be M, internal resistance of the receiver coil be R_2, then the impedance that the load reflects on the feeder is $\omega^2 M^2/(R_2 + R_L)$ [14], [25]. Equivalently, the non-coupling part of the feeder is terminated in an impedance Z'_x as illustrated in Fig. 1(c).

$$Z'_x = Z_0 \tanh(\gamma x) + \frac{\omega^2 M^2}{R_2 + R_L}. \tag{6}$$

The input impedance of the loaded feeder is

$$\begin{aligned} Z_\mathrm{in} &= Z_0 \frac{\tanh(\gamma x) + \tanh[\gamma(L-x)] + \frac{\omega^2 M^2}{Z_0(R_2+R_L)}}{1+\tanh(\gamma x)\tanh[\gamma(L-x)] + \frac{\omega^2 M^2}{Z_0(R_2+R_L)}\tanh[\gamma(L-x)]} \\ &= Z_0 \frac{\sinh(\gamma L) + \frac{\omega^2 M^2}{Z_0(R_2+R_L)}\cosh(\gamma x)\cosh[\gamma(L-x)]}{\cosh(\gamma L) + \frac{\omega^2 M^2}{Z_0(R_2+R_L)}\cosh(\gamma x)\sinh[\gamma(L-x)]} \\ &= Z_0 \tanh(\gamma L) \frac{1 + \frac{\omega^2 M^2}{Z_0(R_2+R_L)} \frac{\cosh(\gamma x)\cosh[\gamma(L-x)]}{\sinh(\gamma L)}}{1 + \frac{\omega^2 M^2}{Z_0(R_2+R_L)} \frac{\cosh(\gamma x)\sinh[\gamma(L-x)]}{\cosh(\gamma L)}} \end{aligned} \tag{7}$$

Because, the characteristic impedance Z_0 is usually large compared to the reflected load $\omega^2 M^2/(R_2 + R_L)$, the term

$\omega^2 M^2/(Z_0(R_2 + R_L))$ is very small compared to one. Exploiting this fact, Z_{in} can be approximated as

$$\begin{aligned} Z_{\text{in}} &\approx Z_0 \tanh(\gamma L)\Bigg\{1 + \ldots \\ &\quad + \frac{\omega^2 M^2 \cosh(\gamma x)}{Z_0(R_2 + R_L)}\left[\frac{\cosh[\gamma(L-x)]}{\sinh(\gamma L)} - \frac{\sinh[\gamma(L-x)]}{\cosh(\gamma L)}\right]\Bigg\} \\ &\approx R_1 + \frac{\omega^2 M^2 \frac{\cosh^2(\gamma x)}{\cosh^2(\gamma L)}}{R_L + R_2} + jX_1 \end{aligned} \tag{8}$$

Obviously, the imaginary part of Z_{in} is equal to that of Z_1 in Eq. (2). Therefore, similar to the unloaded feeder, the loaded feeder is also compensated by the capacitor C_1. As a result, after compensation the input impedance of loaded feeder is purely resistive

$$R_{\text{in}} \approx R_1 + \frac{\omega^2 M^2 \frac{\cosh^2(\gamma x)}{\cosh^2(\gamma L)}}{R_L + R_2}. \tag{9}$$

Based on Eq. (9), a simplified equivalent circuit for the loaded PLF system is described in Fig. 1(d). From this model, the square of kQ-product is derived as a function of location x as follows.

$$\begin{aligned} \chi(x) &\approx \frac{\omega^2 M^2}{R_1 R_2}\left|\frac{\cosh \gamma x}{\cosh \gamma L}\right|^2 \\ &\approx \frac{\omega^2 M^2}{Z_0 R_2}\,\frac{\cosh(2\alpha L) + \cos(2\beta L)}{\sinh(2\alpha L)}\,\frac{\cos^2 \beta x}{\cos^2 \beta L} \\ &\approx \frac{\omega^2 M^2}{Z_0 \alpha L R_2}\cos^2 \beta x \\ &\approx \chi_0 \cos^2 \beta x \end{aligned} \tag{10}$$

where χ_0 is a constant against the receiver position x

$$\chi_0 = \frac{\omega^2 M^2}{Z_0 \alpha L R_2} \tag{11}$$

The overall efficiency of the system is the multiplication of DC-to-RF conversion efficiency at the transmitter, RF-to-RF efficiency of the feeder-receiver pair, and RF-to-DC conversion efficiency at the receiver. These efficiencies in turn depend on the complex impedance of the load. Calculating the overall efficiency is therefore quite complicated as this value depends on many factors. To simplify our analysis, we use the concept of maximum achievable efficiency [22] which is the RF-to-RF efficiency achieved when the load impedance is optimized according to the Z-parameters of the transceiving apparatuses. This value is also a theoretical upper bound on the overall efficiency of the whole system, which is related to the kQ-product as follows.

$$\eta_{\max}(x) = 1 - \frac{2}{1 + \sqrt{1 + \chi(x)}} = 1 - \frac{2}{1 + \sqrt{1 + \chi_0 \cos^2 \beta x}} \tag{12}$$

Equation (12) shows that the maximum efficiency $\eta_{\max}$ vary drastically with the receiver position x, following a standing wave pattern represented by the term $\cos^2 \beta x$. This equation also implies that not the value of R_1 but the term $Z_0 \alpha L$ represents losses in the feeder.

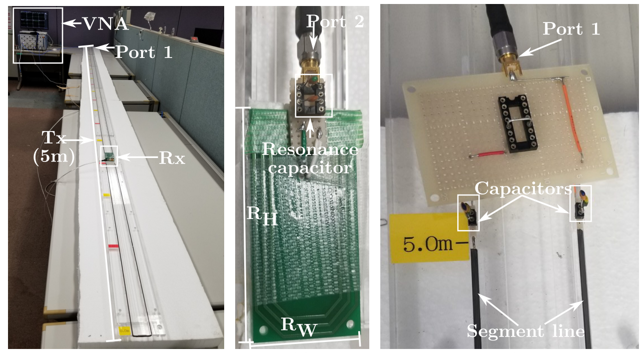

(a) (b) (c)

Fig. 2 Experimental setup.

2.2 Experiments

Experiments are carried out to confirm the theoretical results in Sect. 2.1. The experimental setup of the non-segmented PLF system is shown in Fig. 2(a). In this figure, the feeder is a two-wire transmission line of length $L = 5$ m and width $D = 40$ mm, built from copper wires of diameter $d = 4$ mm and conductivity of 5.8×10^7 S/m. The feeder is terminated in a short-circuit at one end. The other end is connected to port 1 of vector network analyzer (VNA) R&S©ZNBT8. On top of the feeder, a receiver is aligned and is moved from right-hand side to the left-hand side toward the source at a step of 4 cm in the x direction. The air gaps between the feeder and the receiver coil is 2 mm. As shown in Fig. 2(b), the receiver is a spiral coil embeded in a 4 cm × 8 cm printed circuit board (PCB). The receiver coil is connected to the port 2 of the VNA for measurement. All the port impedances are 50 Ω. The IPT system is measured at the operation frequency $f = 27.12$ MHz.

In the unloaded condition, the internal resistance of the feeder and that of the receiver coil are measured as $R_1 = 58.4\ \Omega$ and $R_2 = 1.4\ \Omega$, respectively. In the loaded condition, for each position x of the receiver, we measure the Z-parameters ($Z_{11}, Z_{12}, Z_{21}, Z_{22}$) and calculate the maximum efficiency by using formula given in [21] as follows.

$$\eta_{\text{exp}}(x) = 1 - \frac{2}{1 + \sqrt{1 + \frac{|Z_{21}(x)|^2}{\text{Re}\{Z_1\}\text{Re}\{Z_2\}}}} \tag{13}$$

The measurement results of $\eta_{\text{exp}}(x)$ are shown by the square dots in Fig. 3. Also, this figure shows a fitted curve following Eq. (12) for the measurement results. The fitted curve matches very well with the measurements, indicating that the theoretical formula Eq. (12) accurately reflects the system properties. The curve fitting also yields estimated values for the phase constant $\beta = 0.796$ rad/m and the constant $\chi_0 = 14.74$. Substituting the values of β, χ_0, R_1 and R_2

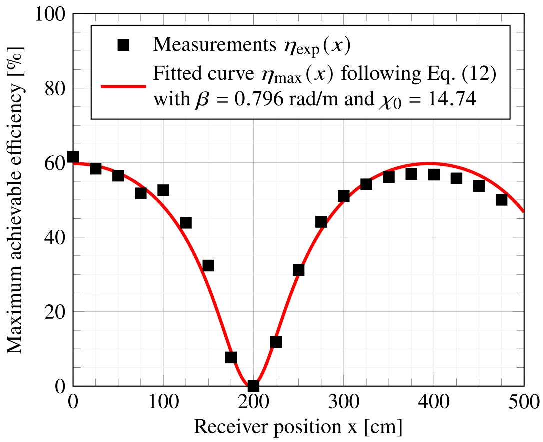

Fig. 3 Maximum achievable efficiency of non-segmented PLF system in Fig. 2 for air gap of 2 mm.

Table 1 Estimated values of non-segmented PLF parameters.

Quantity	Value	
Phase constant β	0.796	[rad/m]
Wavelength $\lambda = 2\pi/\beta$	7.89	[m]
Free-space value of wavelength λ_0	11.05	[m]
Refractive index of dielectric $n = \lambda_0/\lambda$	1.4	
Mutual inductance M	134.1	[nH]
Characteristic impedance $Z_0 = \frac{120\,\Omega}{n}\cosh^{-1}\frac{D}{d}$	357.6	[Ω]

into Eq. (11) we obtain the mutual inductance $M = 134.1$ nH. The wavelength of the signal propagated in the feeder is $\lambda = 2\pi/\beta = 7.89$ m, thus the dielectric of the feeder has a refractive index of $n = 1.4$ and the characteristic impedance of the feeder is $Z_0 = 357.6\ \Omega$. Some parameters for the non-segmented PLF system are summarized in Table 1.

Importantly, Fig. 3 shows that the efficiency drastically varies with the receiver position x following a standing wave pattern. To be specific, the efficiency has a high value when the receiver is at the terminating end $x = 0$. It starts to decrease as the receiver moves toward the power source and becomes zero when the receiver is near the position $x = 200$ cm. The efficiency starts to increase as the receiver moves further toward the source and reaches a highest value when the receiver is near the position $x = 400$ cm. It then again starts to decrease as the receiver moves further toward the source. The drastic variation of efficiency following a standing wave pattern mentioned above limits the deployment of the non-segmented PLF system. This system can not effectively charge receivers at any positions but only the receivers nearby the current anti-nodes, which are periodically separated by a quarter-wavelength.

3. Segmented PLF

3.1 Unloaded Condition

This section presents the segmented PLF which is a modification for the PLF to improve and stabilize the efficiency. The proposed segmented PLF is shown in Fig. 4(a), where

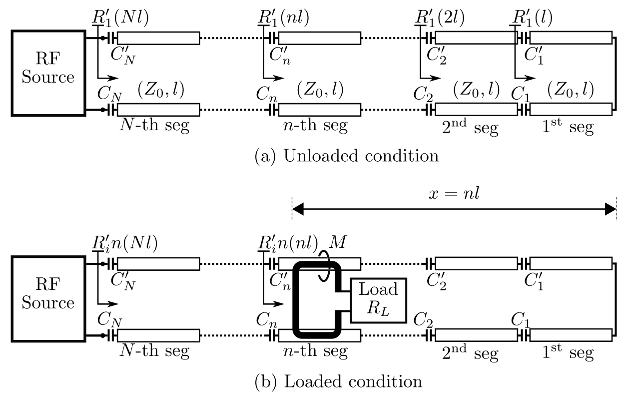

Fig. 4 System model of segmented PLF.

the feeder of length L is equally divided into N segments, each segment has a length of $l = L/N$. The number of total segments N is chosen so that the segment length $l = L/N$ is sufficiently short. The purpose is to guarantee the magnetic field generated by one segment is even and the system efficiency does not significantly change as the receiver coil moves within one segment. Of course, when the receiver coil moves from one segment to another, the system efficiency may vary. The segments are numbered as #n, where $n \in \{1, 2, \ldots, N\}$, and the segment number is increased when going from the right-hand side to the left-hand side. The reactance of each segment is cancelled by two balanced resonant capacitors. To be specific, the n-th segment is compensated by two capacitors C_n and C'_n having similar capacitances.

Let us consider input impedance of the segmented PLF in the unloaded condition in Fig. 4(a). Because the first segment is terminated in a short circuit, its input impedance before compensation by C'_1 is

$$
\begin{aligned}
Z'_1(l) &= R'_1(l) + jX'_1(l) \\
&= Z_0 \tanh(\alpha l + j\beta l) \\
&= \frac{Z_0 \sinh 2\alpha l + jZ_0 \sin 2\beta l}{\cosh 2\alpha l + \cos 2\beta l}
\end{aligned}
\tag{14}
$$

Because the segmentation length l is very short such that $\alpha l \ll 1$, $\sinh(2\alpha l) \approx 2\alpha l$ and $\cosh(2\alpha l) \approx 1$, $Z'_1(l)$ can be approximated as

$$
Z'_1(l) = R'_1(l) + jX'_1(l) \approx \frac{Z_0 \alpha l}{\cos^2 \beta l} + jZ_0 \tan \beta l \tag{15}
$$

The imaginary part $jX'_1(l) = jZ_0 \tan \beta l$ will be compensated for by two balanced capacitors C_1 and C'_1. As a result, the input impedance of the first segment after compensation is a purely real value

$$
R'_1(l) = \mathrm{Re}\{Z'_1(l)\} \approx \frac{Z_0 \alpha l}{\cos^2 \beta l}. \tag{16}
$$

This resistance is the terminating impedance for the second segment, thus the input impedance of the first two segments before compensation is

$$Z_1'(2l) = Z_0\frac{R_1'(l) + Z_0\tanh\gamma l}{Z_0 + R_1'(l)\tanh\gamma l} \tag{17}$$

As the segment length l is very short such that the phase change βl and the attenuation αl are very small, it is obvious that $R_1'(l)$ shown in Eq. (16) is very small compared to the characteristic impedance Z_0. As a result, the input impedance $Z_1'(2l)$ can be approximated as

$$\begin{aligned}
Z_1'(2l) &= R_1'(2l) + jX_1'(2l)\\
&= \frac{R_1'(l) + Z_0\tanh\gamma l}{1 + \frac{R_1'(l)}{Z_0}\tanh\gamma l}\\
&= \frac{R_1'(l) + R_1'(l) + jX_1'(l)}{1 + \frac{R_1'(l)}{Z_0}\tanh\gamma l}\\
&\approx \frac{2R_1'(l) + jZ_0\tan\beta l}{1 + \frac{R_1'(l)}{Z_0}\cdot\frac{R_1'(l)}{Z_0} + j\frac{R_1'(l)}{Z_0}\tan\beta l}\\
&\approx \frac{2R_1'(l) + jZ_0\tan\beta l}{1 + j\frac{R_1'(l)}{Z_0}\tan\beta l}\\
&\approx [2R_1'(l) + jZ_0\tan\beta l]\left[1 - j\frac{R_1'(l)}{Z_0}\tan\beta l\right]\\
&\approx \sum_{m=0}^{2-1}\left[\frac{1}{\cos^2\beta l}\right]^m R_1'(l) + jZ_0\tan\beta l
\end{aligned} \tag{18}$$

The imaginary part of $Z_1'(2l)$ is also $jZ_0\tan\beta l$ which is equal to the reactance of the first segment $jX_1'(l)$. This means the resonant capacitors C_2 and C_2' for the second segment are similar to the resonant capacitors C_1 and C_1' for the first segment. The combined impedance of the first two segments after compensation is purely real

$$R_1'(2l) = \sum_{m=0}^{2-1}\left[\frac{1}{\cos^2\beta l}\right]^m R_1'(l) \tag{19}$$

Similarly, it is obvious that the impedance of the first n segments before the resonant capacitor C_n' is

$$\begin{aligned}
Z_1'(nl) &= R_1'(nl) + jX_1'(nl)\\
&\approx \sum_{m=0}^{n-1}\left[\frac{1}{\cos^2\beta l}\right]^m R_1'(l) + jZ_0\tan\beta l
\end{aligned} \tag{20}$$

As shown in Eq. (20), the reactive component of $Z_1'(nl)$ is

$$X_1'(nl) \approx jZ_0\tan\beta l \tag{21}$$

which is also equal to those of $Z_1'(l)$ and $Z_1'(2l)$. Thus, this component is cancelled by two balanced capacitors C_n and C_n' having the similar capacitances as the compensation capacitors of other segments. Consequently, the impedance of the first n segments after compensation has a purely real value

$$R_1'(nl) \approx \sum_{m=0}^{n-1}\left[\frac{1}{\cos^2\beta l}\right]^m R_1'(l). \tag{22}$$

Eventually, the internal resistance of all the N segments after compensation, which is also the internal resistance of the transmitting coil in the proposed system is

$$\begin{aligned}
R_1' \triangleq R_1'(Nl) &\approx \frac{1 - \left[\frac{1}{\cos^2\beta l}\right]^N}{1 - \frac{1}{\cos^2\beta l}} R_1'(l)\\
&\approx \frac{1 - \left[\frac{1}{\cos^2\beta L/N}\right]^N}{1 - \frac{1}{\cos^2\beta L/N}}\frac{Z_0\alpha L/N}{\cos^2\beta L/N}
\end{aligned} \tag{23}$$

The value of R_1' in Eq. (23) for the special case $N = 1$ is $Z_0\alpha L/\cos^2\beta L$, which is similar to the internal resistance R_1 of the non-segmented PLF in Eq. (3). Because Eq. (23) is not a monotonically increasing function of N, it is hard to say that R_1' decreases immediately from the initial value R_1 when we increase the number of segments N to 2 or 3. However, when N is sufficiently large such that the value of $\cos^2\beta L/N$ approaches 1, the value of R_1' reduces and will approach $Z_0\alpha L$. In such a case, the segmented PLF behaves like a lumped-element and R_1' reflects losses in the loaded condition. A reduction of R_1' therefore pays contribution to efficiency improvement for the segmented PLF. The significance of reducing the feeder resistance is more obvious to this system than to the conventional non-segmented one.

3.2 Loaded Condition

Now, let us consider the segmented feeder in loaded condition illustrated in Fig. 4(b). Without loss of generality, let us assume that the feeder couples with the receiver coil at the n-th segment. In this case, the input impedances of the first, the second, ... and the $(n-1)$-th segments do not change from their values in the unloaded condition in Sect. 3.1. However, the input impedance of the n-th segment changes from Eq. (22) because the load R_L reflects an impedance $\omega^2M^2/(R_2 + R_L)$ onto this segment via the mutual inductance M. As a result, the impedance of the first n-th segments in loaded condition is

$$\begin{aligned}
R_{in}'(nl) &= R_1'(nl) + \frac{\omega^2M^2}{R_2 + R_L}\\
&\approx \sum_{m=0}^{n-1}\left[\frac{1}{\cos^2\beta l}\right]^m R_1'(l) + \frac{\omega^2M^2}{R_2 + R_L}
\end{aligned} \tag{24}$$

In Eq. (24), the first term represents the total internal resistances of the first n segments and the second term represents the reflected impedance of the load onto the feeder.

The $(n+1)$-th segment is terminated in $R_{in}'(nl)$. Therefore, the impedance of the first $(n+1)$ segments including the load can be expressed as follows.

$$\begin{aligned}
Z_{in}'((n+1)l) &= R_{in}'((n+1)l) + jX_{in}'((n+1)l)\\
&= \frac{R_{in}'(nl) + Z_0\tanh\gamma l}{1 + \frac{R_{in}'(nl)}{Z_0}\tanh\gamma l}
\end{aligned} \tag{25}$$

As $R_{in}'(nl) \ll Z_0$ and $Z_0\tanh\gamma l = R_1'(l) + jZ_0\tan\beta l$, we can approximate $Z_{in}'((n+1)l)$ as follows.

$$\begin{aligned} Z'_{\text{in}}((n+1)l) &\approx [R'_1(nl) + R'_1(l) + jZ_0 \tan\beta l] \\ &\quad \times \left[1 - j\frac{R'_1(l)}{Z_0}\tan\beta l\right] \\ &\approx \sum_{m=0}^{n}\left[\frac{1}{\cos^2\beta l}\right]^m R'_1(l) \\ &\quad + \frac{1}{\cos^2\beta l}\frac{\omega^2 M^2}{R_2 + R_L} + jZ_0\tan\beta l \end{aligned} \tag{26}$$

In Eq. (26), the imaginary part will be cancelled by the compensation capacitors C_{n+1} and C'_{n+1}, resulting in a pure resistance

$$R'_{\text{in}}((n+1)l) \approx \sum_{m=0}^{n}\left[\frac{1}{\cos^2\beta l}\right]^m R'_1(l) + \frac{1}{\cos^2\beta l}\frac{\omega^2 M^2}{R_2 + R_L} \tag{27}$$

Eventually, input impedance of the whole segmented feeder in the loaded condition is

$$\begin{aligned} R'_{\text{in}} &\triangleq R'_{\text{in}}(Nl) \\ &\approx \sum_{m=0}^{N-1}\left[\frac{1}{\cos^2\beta l}\right]^m R'_1(l) + \left[\frac{1}{\cos^2\beta l}\right]^{N-n}\frac{\omega^2 M^2}{R_2 + R_L} \\ &\approx \frac{1 - \left[\frac{1}{\cos^2\beta l}\right]^N}{1 - \frac{1}{\cos^2\beta l}} R'_1(l) + \left[\frac{1}{\cos^2\beta l}\right]^{N-n}\frac{\omega^2 M^2}{R_2 + R_L} \\ &\approx R'_1 + \left[\frac{1}{\cos^2\beta l}\right]^{N-n}\frac{\omega^2 M^2}{R_2 + R_L} \end{aligned} \tag{28}$$

From Eq. (28), the kQ-product of this system can be expressed as

$$\chi'(nl) = \frac{\omega^2 M^2}{R'_1 R_2} \cdot \left[\frac{1}{\cos^2\beta l}\right]^{N-n} \tag{29}$$

Thus, the maximum achievable efficiency of the segmented PLF system is given by

$$\eta'_{\max}(nl) = 1 - \frac{2}{1 + \sqrt{1 + \frac{\omega^2 M^2}{R'_1 R_2} \cdot \left[\frac{1}{\cos^2 \beta L/N}\right]^{N-n}}} \tag{30}$$

Equation (30) shows that the efficiency is not a constant but it may slightly vary with n when the receiver moves from one segment to the other. To be specific, the receiver moves to the left-hand side (closer to the source), the maximum efficiency decreases. The efficiency has the highest value when the receiver is at the first segment and has the lowest value when the receiver at the N-th segment. The lowest value of efficiency is an increasing function of the term $\omega^2 M^2/(R'_1 R_2)$. This implies that by sufficiently shortening the feeder length, it is able to reduce the resistance R'_1 and improve the efficiency.

Also in Eq. (30), the magnitude of the term $\cos(\beta L/N)$ decides how drastic the efficiency variation is. When this value is far from 1, the efficiency variation is dynamic, but when this value is close to 1, the efficiency variation is quite slow. Therefore, we can stabilize the system efficiency by using the segmented PLF with a sufficiently shortened segment length l.

4. Experimental Results and Discussions

4.1 Loss Reduction Effect

This section presents experiments with segmented PLF in unloaded condition to show that the losses can be reduced by properly shortening the segment length l. To this end, we fabricate two versions of segmented PLF. The first version has $N = 5$ segments of identical length $l_1 = 1$ m; and the second one has $N = 10$ segments of identical length $l_2 = 0.5$ m. This means both the two segmented versions have the same total length $L = 5$ m as the non-segmented PLF in Sect. 2.2.

Experimental setup of the 5-segment version is shown in Table 2 and that of the 10-segment version is described in Table 3. Table 2 and Table 3 summarize the parameters of the resonant capacitors as well as the impedance of line at each segment before and after inserting the resonant capacitors. We can notice that the capacitors have been chosen to properly cancel the reactive component. Other parameters

Table 2 Added capacitors and input reactance for 5-segment PLF

Segment number n	Length nl	Capacitor (pF) C_n	Capacitor (pF) C'_n	Reactance (Ω) $X'_1(nl)$
1	1	no capacitors		363.4
		30	**29**	**0.8**
2	2	no capacitors		340.9
		35	**35**	**-0.8**
3	3	no capacitors		364.9
		35	**31**	**1**
4	4	no capacitors		367.5
		34	**33**	**-0.8**
5	5	no capacitors		356.8
		36	**36**	**0.5**

Table 3 Added capacitors and input reactance for 10-segment PLF

Segment number n	Length nl	Capacitor (pF) C_n	Capacitor (pF) C'_n	Reactance (Ω) $X'_1(nl)$
1	0.5	no capacitors		107.3
		64	**64**	**1**
2	1	no capacitors		152.5
		76	**76**	**-0.7**
3	1.5	no capacitors		150.2
		79	**82**	**-0.5**
4	2	no capacitors		160.2
		75	**76**	**0.1**
5	2.5	no capacitors		153.2
		80	**77**	**-0.3**
6	3	no capacitors		158.9
		77	**77**	**0.4**
7	3.5	no capacitors		160
		78	**76**	**-0.4**
8	4	no capacitors		159.1
		79	**78**	**0**
9	4.5	no capacitors		157.9
		80	**77**	**-0.1**
10	5	no capacitors		164.9
		76	**76**	**-0.9**

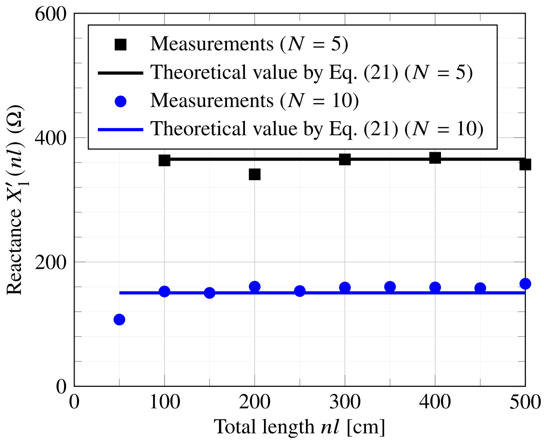

Fig. 5 Reactance of segmented PLF as a function of feeder length.

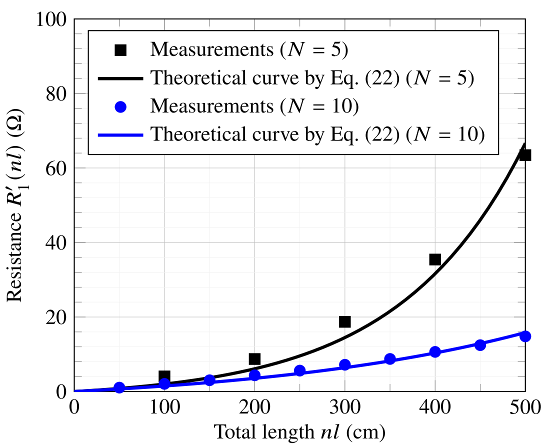

Fig. 6 Resistance of segmented PLF as a function of feeder length.

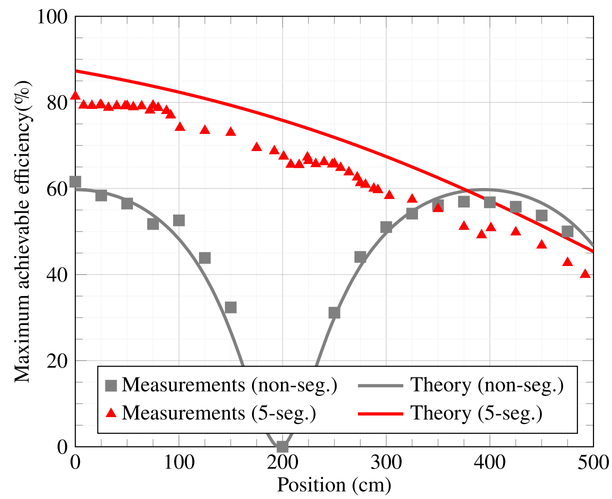

(a) Comparision between 5-segment PLF and non-segmented PLF

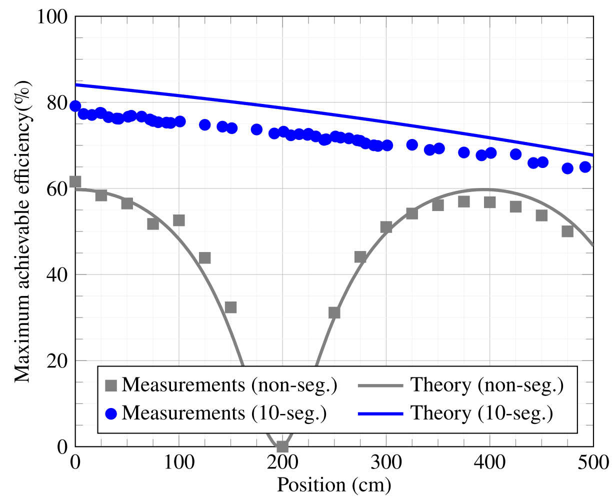

(b) Comparision between 10-segment PLF and non-segmented PLF

Fig. 7 Efficiency comparison for three versions of PLF.

including the wire diameters, the distance between wires, the receiver coil and the operating frequency are the same as of the non-segmented PLF. As for the values of resonant capacitors, there is a good match between the values in Table 2 and Table 3 and the theoretical analysis in Sect. 3. In Table 2, the resonant capacitors have similar values for all 5 segments. In Table 3, except for the first segment, the remaining 9 segments have similar resonant capacitors.

Figure 5 confirms the observation in Eq. (21) that $X'_1(nl) = Z_0 \tan\beta l$ for all $n = 1, 2, \dots N$. The vertical axis of the figure shows the reactance $X'_1(nl)$ for the 5-segment version and the 10-segment version of the PLF. The measurements are shown by the dots; and the theoretical values calculated by Eq. (20) are indicated by the horizontal lines. For the 5-segment version, the measurements are close to the theoretical value of 365.3 Ω. Similarly, for the 10-segment version, the measurements are close to the theoretical value of 150.3 Ω.

Figure 6 verifies the theoretical formula for internal resistance of the segmented PLF shown in Eq. (22). The measurements for the internal resistance are demonstrated by the dots and the theoretical curves by Eq. (22) are expressed by the lines. As shown in the figure, for each version of the feeder, the measurements fit well to the associated theoretical curve; and the internal resistance increases with the total length nl. More importantly, the 10-segment version has a smaller resistance than that of the 5-segment version. The resistance of the 10-segment version is only 14.8 Ω, which is significantly reduced compared to 63.3 Ω resistance of the 5-segment version. This implies that the losses can be significantly reduced by properly shortening the segment length.

4.2 Efficiency Improvement and Stabilization Effects

Using the same receiver coils as in Sect. 2.2, we measure the maximum achievable efficiency for the two versions of the segmented PLF in Sect. 4.1. The air gap between the receiver coil and the feeder is kept unchanged at 2 mm. Following the same process in Sect. 2.2, for each position of the receiver coil along the feeder, we measure the Z-parameters and substitute them into Eq. (13) to calculate the maximum efficiency. The results of this measurement is shown by the triangle dots and circle dots in Fig. 7. This figure also plots theoretical curves for the maximum efficiency by using the measured values of parameters M, β, R_1' and R_2 and by following Eq. (30). In this figure, the measurements and theoretical curve for efficiency of the conventional PLF system are also demonstrated for comparison.

As shown in Fig. 7 (a) for the 5-segment PLF, the measurements agree well with the theoretical curve. Also, it is obvious that the efficiency of the 5-segment PLF does not fluctuates drastically following a standing wave pattern as in the non-segmented one. Even that the 5-segment version exhibits a more stable performance, its efficiency gradually decreases from about 80% to around 40% as the receiver moves from the terminating end toward the source. This characteristic of the segmented PLF agrees with the theoretical analysis in Sect. 3. The efficiency of the 5-segment PLF averaged over all the receiver positions is about 60%. Meanwhile, the non-segmented PLF demonstrates a fluctuation in efficiency between the highest value of around 60% and the lowest value of 0%, meaning its average efficiency over all receiver positions is around 30%. This result confirm that the 5-segment version has a more stable and higher efficiency than the non-segmented one.

Figure 7 (b) shows that the efficiency of the 10-segment version decreases from the highest value of around 80% to the lowest value of about 60%; and the average efficiency over all receiver positions is about 70%. Obviously, the 10-segment PLF exhibits an even more stable and higher efficiency performance compared to the 5-segment version. This result verifies that the efficiency can be improved and stabilized by properly shortening the segment length of the PLF.

5. Conclusions

This paper performed efficiency analysis for segmented PLF system which has been proposed for wireless charging of multiple receivers located in linear topology. Our theoretical analysis has shown that efficiency improvement and stabilization effects can both be achieved provided that the segment length is properly shortened to avoid standing wave problem as well as copper and/or dielectric loss. Experimental results at operating frequency of 27.12 MHz confirm the theoretical analysis and show that the segmentation can stabilize the efficiency as high value as 70% for all receiver positions along the feeder.

Acknowledgments

This work was supported by JSPS KAKENHI Grant Number 19K04376.

References

[1] Z. Zhang, H. Pang, A. Georgiadis, and C. Cecati, "Wireless power transfer-an overview," IEEE Trans. Ind. Electron., vol.66, no.2, pp.1044–1058, Feb. 2019.
[2] L. Xie, Y. Shi, Y.T. Hou, and A. Lou, "Wireless power transfer and applications to sensor networks," IEEE Wirel. Commun., vol.20, no.4, pp.140–145, Aug. 2013.
[3] N. Shinohara, "Trends in wireless power transfer: WPT technology for energy harvesting, mllimeter-wave/THz rectennas, MIMO-WPT, and advances in near-field WPT applications," IEEE Microw. Mag., vol.22, no.1, pp.46–59, Jan. 2021.
[4] B.M. Adarsha, S. Prakash, V.G. Naik, and K.V. Reddy, "Wireless power transfer for wireless sensor networks using hybrid algorithm," International Conference on Computing Methodologies and Communication, pp.68–72, 2017.
[5] S. He, J. Chen, F. Jiang, D.K.Y. Yau, G. Xing, and Y. Sun, "Energy provisioning in wireless rechargeable sensor networks," IEEE Trans. Mob. Comput., vol.12, no.10, pp.1931–1942, Oct. 2013.
[6] Y. Peng, Z. Li, W. Zhang, and D. Qiao, "Prolonging sensor network lifetime through wireless charging," IEEE Real-Time Systems Symposium, pp.129–139, 2010.
[7] T. Ajmal, D. Jazani, and B. Allen, "Design of a compact RF energy harvester for wireless sensor networks," IET Conf. Wireless Sensor Systems (WSS), pp.1–5, London, UK, June 2012.
[8] W.C. Brown, "The history of power transmission by radio waves," IEEE Trans. Microw. Theory Tech., vol.32, no.9, pp.1230–1242, Sept. 1984.
[9] B. Strassner and K. Chang, "Microwave power transmission: Historical milestones and system components," Proc. IEEE, vol.101, no.6, pp.1379–1396, June 2013.
[10] PowerCast Corp., available http://www.powercastco.com
[11] A.P. Sample, D.J. Yeager, P.S. Powledge, A.V. Mamishev, and J.R. Smith, "Design of an RFID-based battery-free programmable sensing platform," IEEE Trans. Instrum. Meas., vol.57, no.11, pp.2608–2615, Nov. 2008.
[12] M. Fantuzzi, M. Del Prete, D. Masotti, and A. Costanzo, "Quasi-isotropic RF energy harvester for autonomous long distance IoT operations," 2017 IEEE MTT-S International Microwave Symposium (IMS), pp.1345–1348, 2017.
[13] Z. Popovic, "Far-field wireless power delivery and power management for low-power sensors," IEEE Wireless Power Transfer Conference, pp.1–4, Perugia, Italy, May 2013.
[14] G.A. Covic and J.T. Boys, "Inductive power transfer," Proc. IEEE, vol.101, no.6, pp.1276–1289, June 2013.
[15] A. Kurs, A. Karalis, R. Moffatt, J.D. Joannopoulos, P. Fisher, and M. Soljačić, "Wireless power transfer via strongly coupled magnetic resonances," Science, vol.317, no.5834, pp.83–86, July 2007.
[16] W.Y. Lee, J. Huh, S.Y. Choi, X.V. Thai, J.H. Kim, E.A. Al-Ammar, M.A. El-Kady, and C.T. Rim, "Finite-width magnetic mirror models of mono and dual coils for wireless electric vehicles," IEEE Trans. Power Electron., vol.28, no.3, pp.1413–1428, March 2013.
[17] U.-M. Jow and M. Ghovanloo, "Geometrical design of a scalable overlapping planar spiral coil array to generate a homogeneous magnetic field," IEEE Trans. Magn., vol.49, no.6, pp.2933–2945, June 2013.
[18] Q. Zhu, L. Wang, Y. Guo, C. Liao, and F. Li, "Applying LCC compensation network to dynamic wireless EV charging system," IEEE Trans. Ind. Electron., vol.63, no.10, pp.6557–6567, Oct. 2016.
[19] J. Li, F. Yin, L. Wang, B. Cui, and D. Yang, "Electromagnetic induction position sensor applied to anti-misalignment wireless charging for UAVs," IEEE Sens. J., vol.20, no.1, pp.515–524, Jan. 2020.
[20] X. Dang, P. Jayathurathnage, S.A. Tretyakov, and C.R. Simovski, "Self-tuning multi-transmitter wireless power transfer to freely positioned receivers," IEEE Access, vol.8, pp.119940–119950, 2020.
[21] V.K. Srivastava, A. Sharma, and A. Bharadwaj, "A planar distributed multicoil antenna to generate 3-D ellipsoidally polarized H-field for angular misalignment tolerant WPT system," IEEE Trans. Antennas Propag., vol.70, no.4, pp.2969–2978, April 2022.
[22] M. Zargham and P.G. Gulak, "Maximum achievable efficiency in

near-field coupled power-transfer systems," IEEE Trans. Biomed. Circuits Syst., vol.6, no.3, pp.228–245, June 2012.
[23] T. Ohira, "Maximum available efficiency formulation based on a black-box model of linear two-port power transfer systems," IEICE Electron. Express, vol.11, no.13, pp.1–6, July 2014.
[24] T. Ohira, "Extended k-Q product formulas for capacitive- and inductive-coupling wireless power transfer schemes," IEICE Electron. Express, vol.11, no.9, pp.1–7, April 2014.
[25] T. Ohira, "Power transfer theory on linear passive two-port systems," IEICE Trans. Electron., vol.E101-C, no.10, pp.719–726, Oct. 2018.
[26] T. Higashino, M. Ziji, M. Okada, Y. Tatsuta, Y. Goto, Y. Tsuruda, and R. Tanaka, "A new configuration of magnetic coupled power transfer using parallel line feeder," IEEE Wireless Power Transfer Conference, pp.171–174, Perugia, Italy, May 2013.
[27] Qi standard, available https://www.wirelesspowerconsortium.com/qi/
[28] Q.T. Duong and M. Okada, "Inductive power transmission using multiple concatenated parallel-line-feeder segments," IEEE Wireless Power Transfer Conference, Aveiro, Portugal, May 2016.
[29] W.-F. Brou, Q.T. Duong, and M. Okada, "Experimental evaluation of inductive power transfer system using multiple concatenated parallel-line-feeder segments," International Symposium on Antennas and Propagation, Okinawa, Japan, Oct. 2016.
[30] D.M. Pozar, Microwave Engineering, 4th ed. John Wiley & Sons, Nov. 2011.
[31] W.M. Middleton and Mac E. Van Valkenburg, Reference Data for Engineers: Radio, Electronics, Computers and Communications, 9th ed. Elsevier Science, 2002.

William-Fabrice Brou received the M.E. degree from the Nara Institute of Science and Technology, Japan, in 2016. He is currently pursuing the Ph.D. degree with the Nara Institute of Science and Technology, Japan. His research interests include wireless power transfer, simultaneous wireless and information transfer and software defined radio.

Quang-Thang Duong received the B.E., M.E., and Ph.D. degrees in communications engineering from Osaka University, Osaka, Japan, in 2009, 2011, and 2014, respectively. He is currently an Assistant Professor with the Nara Institute of Science and Technology. His research interests include broadband wireless access techniques, channel estimation, information theory, error correcting code, wireless power transfer, and simultaneous wireless information and power transfer. He is a member of the Institute of Electrical, Information and Communication Engineers (IEICE) and the Institute of Electrical and Electronics Engineers (IEEE). He is the recipient of the Young Engineer Award and the Michiyuki Uenohara Memorial Award from the IEEE Microwave Theory and Techniques Society (IEEE-MTTS) Japan Chapter in 2019.

Minoru Okada received the B.E. degree from the University of Electro-Communications, Tokyo, Japan, in 1990, the M.E. and Ph.D. degrees from Osaka University, Osaka, Japan, in 1992 and 1998, respectively, all in communications engineering. In 2000, he joined the Graduate School of Information Science, Nara Institute of Science and Technology, Nara, Japan, as an Associate Professor and became a Professor. From 1993 to 2000, he was a Research Associate with Osaka University. From 1999 to 2000, he was a Visiting Research Fellow with the University of Southampton, Southampton, U.K. His research interest is wireless communications, including WLAN, WiMAX, CDMA, OFDM, and satellite communications. He was a recipient of the Young Engineer Award from the Institute of Electrical, Information, and Communication Engineers (IEICE) in 1999. He is a member of the Institute of Television Engineers of Japan, IEICE of Japan, and the Information Processing Society of Japan.